Additive Manufacturing 69 (2023) 103518

Contents lists available at ScienceDirect

Additive Manufacturing

journal homepage: www.elsevier.com/locate/addma

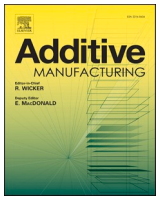

Adding functionality to powder bed fusion materials: Creating magnetic polymers using hybridized hollow carbon nanofibres

Ruth D. Goodridge [a,*,1], Carlos Herreros-Lucas [b,c,1], Maria del Carmen Gimenez-Lopez [b,c,**]

[a] Centre for Additive Manufacturing, School of Engineering, The University of Nottingham, Jubilee Campus, Nottingham NG7 2GX, UK
[b] School of Chemistry, The University of Nottingham, University Park, Nottingham NG7 2RD, UK
[c] CiQUS, Universidad de Santiago de Compostela, 15782 Santiago de Compostela, Spain

ARTICLE INFO

Keywords:
Additive manufacturing
Powder bed fusion
Laser sintering
Polymer nanocomposites
Magnetic properties

ABSTRACT

A method is presented, using Fe_3O_4 nanoparticles hybridized with hollow carbon nanofibers (Fe_3O_4NP@CNF) as an example, to add functionality to polymer powders for powder bed fusion with laser beam (PBF/LB-P). There are currently only a small number of polymers that can be processed successfully and reliably by PBF/LB-P. It was proposed that coating PA12 powder, a material that has a good track record in laser sintering, with a small amount (0.1 wt%) of Fe_3O_4@CNF would provide a new material with additional functionality without affecting the processability of the PA12 powder, since the Fe_3O_4 is contained within the CNF. Commercial PBF/LB-P PA12 particles were coated with Fe_3O_4@CNF without altering the morphology of the powder particles. No significant reduction in the PBF/LB-P processing window was observed when processing the resulting polymer nanocomposites, and parts were produced with comparable mechanical properties to the base polymer. Interestingly, magnetic investigations of PBF/LB-P cylinders built in three different orientations, with alignment of the long symmetry axis along the X, Y or Z axes of the build chamber, showed a preferential orientation of the hybridized magnetic fibers along the Z-axes in the composite. This suggests the appealing possibility of tailoring pieces with preferential magnetic orientation. Moreover, no agglomeration or nanoparticle growth was observed after PBF/LB-P. It is proposed that the low-cost method used in this work could be easily applied to other nanoparticles, without creating restrictive processing windows and the time-consuming process to determine them. Thus, a range of powders with additional functionality could be easily created for use in a variety of applications and industries.

1. Introduction

Additive Manufacturing (AM; commonly referred to as 3D-Printing) is increasingly being used in a variety of high-value industries due to the advantages it offers in terms of increased design freedom, reduced cost of customization, on-demand manufacture, reduced manufacturing and assembly steps [1]. Polymer powder bed fusion with laser beam (PBF/LB-P) techniques, such as laser sintering, are of particular interest to industry as they allow complex objects to be produced that are difficult or impossible to process using other AM techniques, as they do not require the use of support structures for overhanging and isolated sections of the part being built. This provides designers with significantly increased design freedom and the opportunity to stack parts within a build volume allowing for more efficient manufacture [2].

However, there are currently only a small number of polymers that can be processed successfully and reliably by PBF/LB-P. There are difficulties in increasing the number of polymers for PBF/LB-P due to complex heating and cooling effects (in process and post-process) [3,4]. For each new material, a "processing window" must be established, which includes determining the range of heating and cooling rates, temperatures and patterns, in combination with laser scanning parameters such as laser power, scan speed, scan overlap etc, that can be used to successfully produce parts. For the commonly used polyamide 12 (PA12), which has a relatively wide processing window, allowing a

* Corresponding author.
** Corresponding author at: CiQUS, Universidad de Santiago de Compostela, 15782 Santiago de Compostela, Spain.
E-mail addresses: ruth.goodridge@nottingham.ac.uk (R.D. Goodridge), carlos.herreros@usc.es (C. Herreros-Lucas), maria.gimenez.lopez@usc.es (M. del Carmen Gimenez-Lopez).
[1] joint first author.

https://doi.org/10.1016/j.addma.2023.103518
Received 30 September 2022; Received in revised form 10 February 2023; Accepted 20 March 2023
Available online 30 March 2023

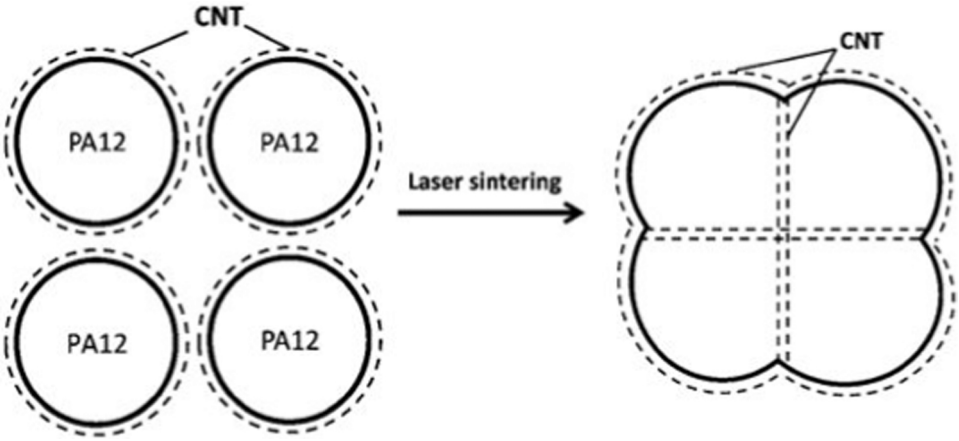

Fig. 1. Schematic explanation of consolidation by PBF/LB-P of polymer powder particles (PA12) coated with carbon nanotubes (CNTs) from our previous study; dash lines represent the CNTs [9].

range of thermal and scanning combinations to be used, this is well established and whilst some tweaking of the exact parameters may be needed for different machines, the effects of changing parameters are relatively well known. However, when developing new materials, these parameter sets need to be established, usually using a trial-by-error method, which is time-consuming and costly. In addition, as most materials do not process as easily as PA12, complex scan strategies may need to be explored, which can be geometry dependent and require intelligent scan patterns. Even with intelligent scan strategies, many materials will simply not process consistently enough for use in commercial activities.

One way to increase the functionality of laser sintering materials is to combine PA12, which has good processability by PBF/LB-P (and an established history of use), with a functional material, thus creating a PA12 nanocomposite.

A number of researchers have processed polymer nanocomposites by PBF/LB-P. However, common challenges include ensuring good dispersion of the nanoparticles [5,6] and preparing polymer nanocomposite powders with suitable morphology for PBF/LB-P [7]. To address this, we previously proposed the use of a simple, low-cost method to coat the individual PA12 particles with a small amount (0.1 wt%) of carbon nanotubes prior to processing [8,9]. This method allows the carbon nanotubes to be uniformly distributed throughout the laser sintered structures. In PBF/LB-P, only the surface of the polymer powder particle tends to melt [10], and thus a network of carbon nanotubes at the particle boundaries in the processed part result, spaced apart by approximately the diameter of the powder particle (typically around 50 μm) (Fig. 1).

In our prior work, using just 0.1 wt% CNTs resulted in increases of 54% in Young's Modulus, 6.2% in ultimate tensile strength (UTS), 13.0% in flexural modulus, 10.9% in flexural strength and 123.9% in impact strength, without sacrificing elongation at break [8]. This low volume of nanofiller, coupled with the simple method to prepare the nanocomposite, combine to make it a cost-effective way to prepare polymer nanocomposites that can have a significant effect on the resulting properties.

In our current study, we aimed to demonstrate additional functionality through the use of hybrid metal-carbon nanomaterials. Our aim was not to develop a new material and demonstrate its use in a particular application. Instead, our aim was to demonstrate how we can easily enhance the functionality of PA12 powder particles using a low-cost method that does not significantly reduce the processing window or require a separate processing window to be found, a procedure that is time-consuming and costly. It is envisaged that this method can be used to create a range of PBF/LB-P powders with different functionalities, quickly and cheaply, by changing the nanoparticle that is hybridized with carbon nanofibers (CNFs). To avoid previous issues with some functional nanoparticles interacting with the laser and negatively affecting the processing window [11], we propose the encapsulation of such functional nanomaterials (i. e. nanoparticles) inside carbon nanofibers (CNFs) [12]. In addition to their lower cost, in previous work, we have demonstrated that the wider internal cavity of CNFs, with respect to CNTs [13], facilitates the encapsulation of functional nanoparticles and stabilizes them even under harsh conditions [14–16].

To demonstrate the concept, we sought to create a magnetic PBF/LB-P powder that could be potentially used in a variety of applications, for example to produce motors or magnetically driven healthcare devices, devices that are externally actuated with an alternating magnetic field to control movement or generate localized heating [17,18]. However, this functionality was chosen just as proof of concept, to demonstrate the ability to fill carbon structures with a secondary phase that would offer an additional function whilst not requiring a new processing window to be determined.

We selected magnetic Fe_3O_4 nanoparticles because magnetite (Fe_3O_4) has, after pure iron, the best ferromagnetic properties among the minerals found in nature [19]. Note that the synthesis of magnetic composites is currently a challenge because of the strong tendency of the nanoparticles to agglomerate. Previous attempts by Wu et al. to create magnetic sintered composites relied on the use of non-magnetic powder, to avoid the agglomeration phenomenon when creating the composites, which was magnetized in a subsequent step [20]. Hupfeld et al. have previously investigated PBF/LB-P of polyamide particles coated with iron oxide nanoparticles using laser fragmentation in liquids (LFL) and a colloidal additivation process [21]. They reported that only minor aggregation was observed and the material had "good processibility", although a direct comparison to the processing window of the base polymer was not made. However, mechanical properties were not included, and it was not clear whether the process window had to be re-established for the nanocomposite powder. In preparation of the powder, they did not appear to be able to control the nanoparticle morphology nor the chemical composition, since a very polydiverse sample of nanoparticles was obtained after LFL and a partial reduction of the maghemite educt material occurred. The authors concluded that the magnetic properties of the nanoparticles were successfully transferred to the final part, however, as FeO_x was used, this is perhaps not entirely relevant. Dusenberg et al. synthesized Fe_3O_4 nanoparticles using a simpler, co-precipitation method [22].

However, they also had issues controlling the final morphology and composition of the particles, and a polydiverse sample was used, with nanoparticle size between 10 and 20 nm. They found it difficult to disperse the Fe_3O_4 nanoparticles on the polymer surface even when adding surfactants such as oleic acid. They reported that most Fe_3O_4

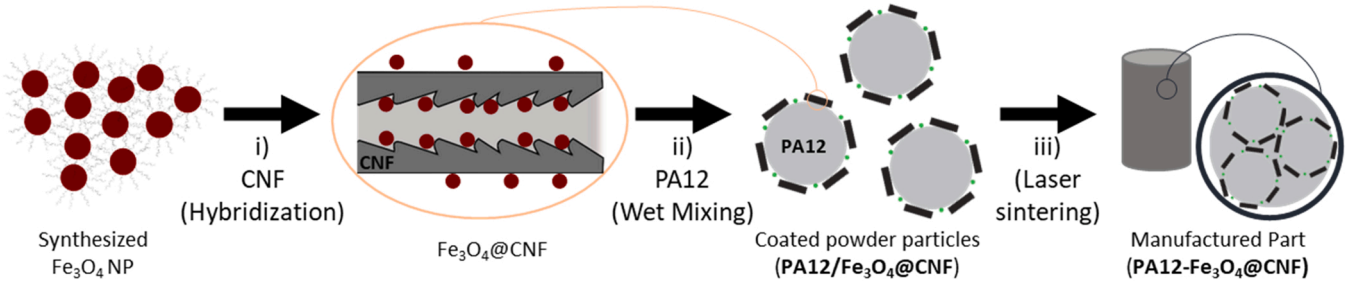

Fig. 2. Schematic of the process used to produce PBF/LB-P parts (PA12-Fe_3O_4@CNF) from PA12 coated with Fe_3O_4 nanoparticles hybridized with hollow carbon nanofibers (Fe_3O_4@CNF) by three-step: i) hybridization of nanoparticles with carbon nanofibers, ii) coating of PA12 microparticles with Fe_3O_4@CNF (PA12/Fe_3O_4@CNF) and iii) PBF/LB-P of a manufactured part in the desired design (i. e. cylinder). Green dots refer to TiO_2.

particles were present in agglomerates larger than 100 nm.

In the work presented in this paper, PA12 particles were coated with 0.1 wt% hybrid carbon nanomaterials (Fe_3O_4@CNF) to produce PA12/Fe_3O_4@CNF powder which was then consolidated in PA12-Fe_3O_4@CNF composite by laser sintering on an industrial CO_2 laser based system (EOS P100) (Fig. 2). PA12 (EOS PA2200) was used as the base polymer for proof of concept due to its established use in laser sintering; however, it is envisaged that this method could be applied to other laser sintering polymers.

This approach, (i.e., the encapsulation of Fe_3O_4 nanoparticles inside one-dimensional CNF containers, rather than simply using Fe_3O_4 nanoparticles), was designed to overcome the limitations reported in previous work. It was proposed that nanoparticle agglomeration during PBF/LB-P would be hindered by the encapsulation of Fe_3O_4 nanoparticles within carbon nanofibers [23]. Furthermore, it has been demonstrated that lasers can be employed to grow and modify Fe_3O_4 NP [24,25]. It was proposed that using CNFs as protective containers would avoid any morphological and chemical changes on the nanoparticles triggered by the laser during processing that could affect their magnetic behaviour. This was proposed based on the previous work of the authors in which it was demonstrated that nanoparticles confined in CNFs can retain their small size, and hence their properties, even under very harsh temperature conditions [26]. In addition, the proposed method sought to prevent the need to find a new processing window each time new functionality is required, and to ensure mechanical properties are not reduced. Lastly, a low cost method of coating commercially available powder was desired so that small batches of powder with different functionalities could be easily produced with no specialized equipment, and no changes to the powder shape and size.

2. Experimental section

2.1. Materials

Polyamide 12 (PA12) powder was supplied by EOS GmbH (Germany), trade name PA 2200. Graphitised carbon nanofibres (PR-24-XT-HHT, produced by chemical vapour deposition, length is in the range of 50–200 μm, average inner and outer diameter are ~30 and ~100 nm, respectively). All other reagent and solvents were purchased from Sigma-Aldrich, UK and used without further purification. Commercial dispersant used to form aqueous carbon nanofiber suspensions was supplied by NanoLab Inc. (USA), trade name Nanosperse AQ.

2.2. Preparation of Fe_3O_4NP@CNF [21]

100 mg of 4-nm Fe_3O_4 nanoparticles obtained following Sun et al. procedure [27] were suspended in 50 mL of hexane and sonicated for 15 min 100 mg of pre-heated PR24 carbon nanofibres (300°C, 30 min) were added to the dark suspension and sonicated for 15 min. After removing the solvent under reduced pressure, 25 mL of hexane were added to the flask and sonicated for 15 min. The process was repeated 5 times. Finally, the suspension was filtered through PTFE membrane and washed thoroughly with hexane, yielding 96 mg, with around a 10% of nanoparticles loading.

2.3. Preparation of PA12-Fe_3O_4NP@CNF

Two nanocomposite powders were prepared: 1) Polyamide 12 reinforced with carbon nanofibers (PA12-CNF); 2) Polyamide 12 reinforced with iron oxide-filled carbon nanofibers (PA12- Fe_3O_4@CNF). Both materials were prepared by coating the individual PA12 particles with the nanophase, using a method which maintains the near-spherical morphology of the as-supplied powder which is ideal for PBF/LB-P. Briefly, the carbon nanofibers were initially suspended in water with the dispersant and ultrasonicated in order to form a 1.0 wt% aqueous suspension of individual particles. These suspensions were used to coat the polymer particles giving a nanocomposite with 0.1 wt% CNF (or Fe_3O_4@CNF) load.

2.4. Characterisation of preformed nanoparticles and hybrid materials

HRTEM images measurements were performed using a Jeol 2100 F transmission electron microscope at an accelerating voltage of 200 kV. TEM specimens were prepared by casting several drops of a suspension of the carbon material in hexane onto a copper-grid mounted “holey” carbon film before drying under a stream of nitrogen. SEM images were acquired on a field emission scanning electron microscope (XL30 FESEM) with 15 kV working voltage. A Nicolet Avatar 380 FT-IR spectrometer was used to measure Infra-red spectra over the range 400–4000 cm^{-1}. Raman samples were measured in solid state under ambient conditions with a WiTec alpha300 series Raman spectrometer. TGA was carried out on a SDT Q-600 TA instrument over the range of 25–1000 °C in air with a scan rate of 5 °C/min. Powder XRD patterns were recorded using a PANalytical diffractometer equipped with Cu Kα source ($\lambda = 1.5418$ Å).

2.5. Characterisation of the prepared powders

The transition temperatures of the powders were studied on a DSC instrument (Q200-TA). The tests were performed in an inert gas atmosphere and included a heating step from 25 °C to 200 °C and a cooling step from 200 °C to 25 °C, both at a heat exchange rate 5 °C/min. Samples ranging between 4.4 mg and 4.6 mg were used.

2.6. Processing of the nanocomposite by laser sintering

The two polymer nanocomposites, along with a non-filled PA12 material that was used as a control, were processed by PBF/LB-P on an EOS P100 machine. The laser sintering processing parameters used for all three materials were 175 °C (bed temperature), 0.25 mm scan spacing, 0.1 mm layer thickness, 2500 mm/s scan speed, 21 W laser power. Additional tensile test specimens were fabricated using

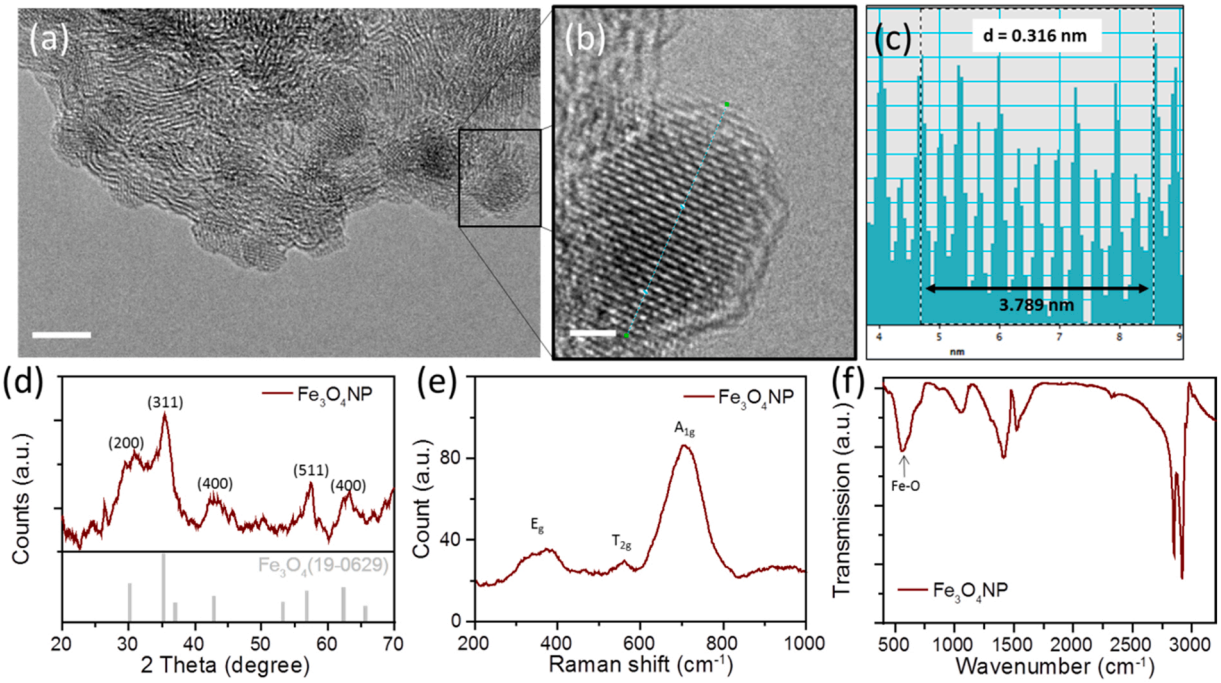

Fig. 3. Structural characterization of preformed Fe_3O_4 nanoparticles. (a) TEM image of spherical Fe_3O_4 NPs with a size distribution of 4.3 ± 1.1 nm (Fig. S1), (b) High-resolution TEM image where the interplanar spacing (d = 0.316 nm) of the particle in b shows a good agreement with that of the Fe_3O_4 200 plane. Interplanar spacing (c) is calculated as d = L/(N-1) being L the total length (i.e. 3.789 nm) and N the number of layers (i.e. 13). (d) XRD pattern, (e) Raman and (f) IR spectrum of preformed Fe_3O_4 NP. Scale bars are 5 (a) and 2 (b) nm.

2000 mm/s scan speed (all other parameters the same) and 25 W laser power (all other parameters the same). SQUID tests specimens were designed as cylinders, 4 mm diameter by 10 mm height, built in three orientations with alignment of the long symmetry axis along the X, Y and the Z axes of the build chamber.

Functional Magnetic Characterization of laser sintered parts.

Commercial Quantum Desing MPMS-XL5 Superconducting Quantum Interference Device (SQUID) magnetometer was employed to measure the magnetic measurements of Fe_3O_4 nanoparticles, Fe_3O_4@CNF hybrid and PA12-Fe_3O_4@CNF sintered parts. A plastic capsule with a negligible diamagnetic contribution was used for carefully measuring Fe_3O_4 NP and Fe_3O_4@CNF samples, while specimens of PA12-Fe_3O_4@CNF were cylinder shaped with diameter of 6 mm and height of 10 mm. Variable-temperature (2–300 K, with 0.5 T and 0.1 T applied field) and field dependent (0–5 T, at 2 and 300 K) magnetisation measurements, and alternating current (AC) measurements (at different frequencies (1–997 Hz) of a 3.5 Oe oscillating field between 15 and 50 K) were carried out. The observed time dependence on temperature for the in-phase χ'signal for Fe_3O_4NP, Fe_3O_4@CNF and PA12-Fe_3O_4@CNF was analysed on the basis of a noninteracting system (i.e. Arrhenius law) and interacting systems (i.e. Vogel-Fulcher law). For nanoparticles the values for the time constant τ_0 are between 10^{-9} and 10^{-13} s.

2.7. Characterisation of laser sintered parts

The morphology of the nanocomposites was studied by scanning electron microscopy (SEM) on a ZEISS FESEM ULTRA Plus with EDX. DSC measurements were carried out using a TA Instruments Q200 system.

2.8. Mechanical testing of laser sintered parts

Tensile testing was performed according to BS EN ISO 527 on an Instron Universal 5985 machine equipped with a 5 kN load cell and an Imetrum video gauge extensometer, at an uniaxial pulling speed 10 mm min^{-1}. Notched Izod impact tests were completed on an Avery machine as an average value from 5 specimens prepared according to the BS EN ISO 180 standard.

2.9. Confocal Raman spectroscopy

High spatial resolution Raman scattering imaging was performed using a commercial confocal Raman microscope, WITec alpha300 RA. The microscope has an ultra-high throughput spectrometer with 1800 g/mm grating and a back-illuminated electron-multiplied CCD camera detector. An XY(Z) piezo stage controls the movement of the sample in a few nm precision. A laser excitation wavelength of 532 nm was utilized in this work. No sample preparation was required for the analysis of the laser sintered composite.

3. Results and discussion

3.1. Preparation of Fe_3O_4 nanoparticles hybridized with hollow carbon nanofibers (Fe_3O_4@CNFs)

Preformed magnetite (Fe_3O_4) nanoparticles were synthesized using a standard protocol in which $Fe(acac)_3$ is thermally decomposed in high boiling organic solvent, being the morphology selectively controlled by the presence of surfactants (i.e. oleic acid and oleylamine) [27]. Magnetite (Fe_3O_4) crystal, which has an inverse spinel structure with alternating octahedral and tetrahedral layers, shows interesting magnetic and electrical properties because of transfer of electrons between Fe^{2+} and Fe^{3+} ions present in octahedral sites [28].

It is important to synthesize iron oxide nanoparticles with a specific phase composition, as well as a narrow size distribution, as these parameters determine their magnetic behaviour [19,29]. In the case of Fe_3O_4 NP, size is greatly relevant, for example they show ferromagnetic behaviour at large sizes (i. e. higher than 20 nm), while at smaller sizes (lower than 20 nm) they exhibit superparamagnetic properties [30].

The hydrothermal method employed in this study, which is based on

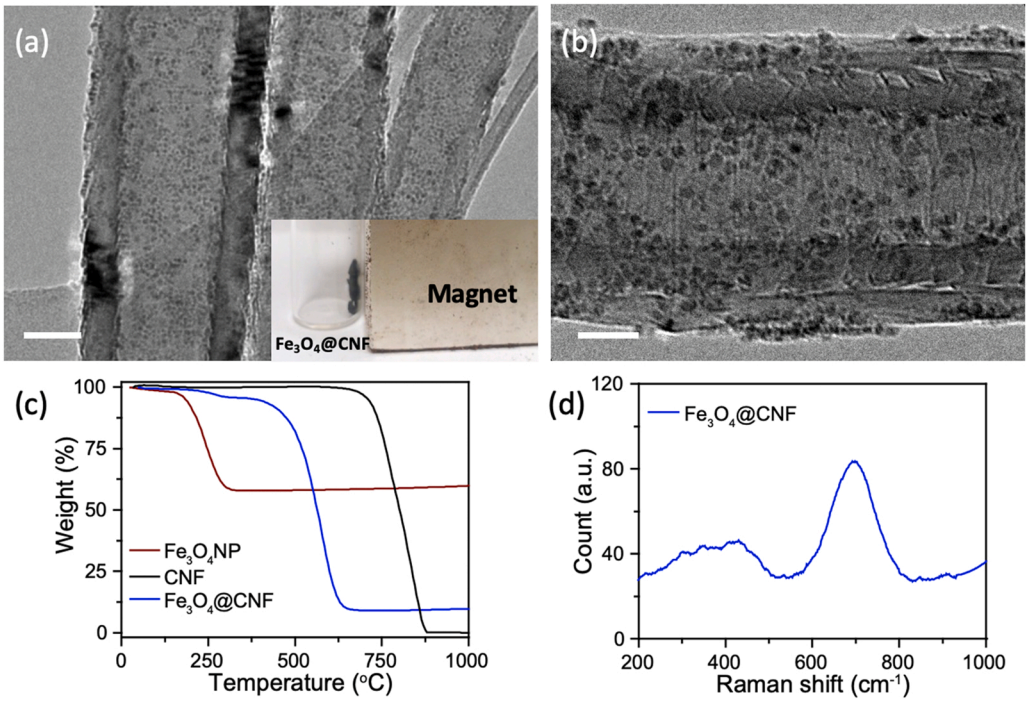

Fig. 4. Structural characterization of Fe_3O_4 nanoparticles in tubular carbon nanofibers (Fe_3O_4@CNF). (a-b) TEM micrographs of Fe_3O_4@CNF hybrid. (c) TGA of preformed nanoparticles (Fe_3O_4 NP), pristine hollow carbon nanofibers (CNF) and hybrid material (Fe_3O_4@CNF) at 5 °C/min in air. (d) Raman spectrum of hybrid material confirming peaks of Fe_3O_4 located at 318–431 and 691 cm^{-1}. Scale bars are 50 (a) and 20 (b) nm. (a, inset) Fe_3O_4@CNF close to a neodymium magnet of 0.1 strength.

the thermal decomposition of an organometallic precursor (iron (III) acetylacetonate) in the presence of surfactants, is known to be very effective on selectively controlling the composition and morphology of nanoparticles, which are key factors for addressing magnetic applications [31]. Both the average size and the size distribution of the pseudospherical (anisotropic) nanoparticles closely depend on nucleation rate and growth. These can be controlled by selecting the reaction temperature and the surfactants concentration [32]. Thus, by using this methodology we produced free-standing monodispersed pseudospherical nanoparticles with control of their composition and size, and therefore their magnetic properties. Another advantage of this method is that the resulting free-standing nanoparticles are not only hydrophobic (i. e. because of the hydrophobic capping layer), but also very small (< 10 nm), which is very beneficial for their encapsulation within the hollow carbon nanofibers, as well as improving the interaction with the hydrophobic carbon surface [26,33]. Although easier synthetic methods (i. e. precipitation method from aqueous systems) may be employed, key important parameters for magnetic applications such as the size, shape or phase composition are often difficult to control [34]. Moreover, the synthesis of nanoparticles covered by a hydrophobic capping layer (such as the one reported in our study) using this precipitation method usually would require a subsequent second step for the surface modification, employing amphiphilic surfactants [35,36].

Confirmation of the chemical composition and structure of the preformed magnetite nanoparticles (Fe_3O_4) was obtained by several techniques such as high-resolution transmission electron microscopy

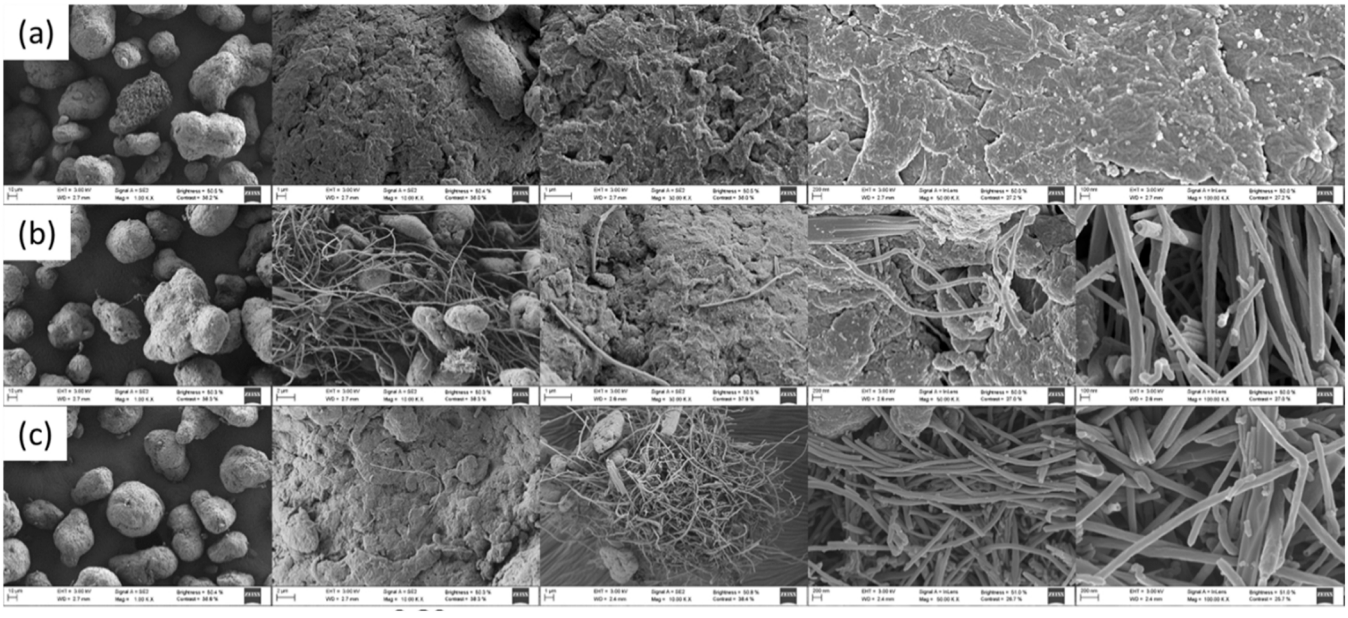

Fig. 5. SEM images of (a) PA12, (b) PA12/CNF and (c) PA12/Fe_3O_4@CNF.

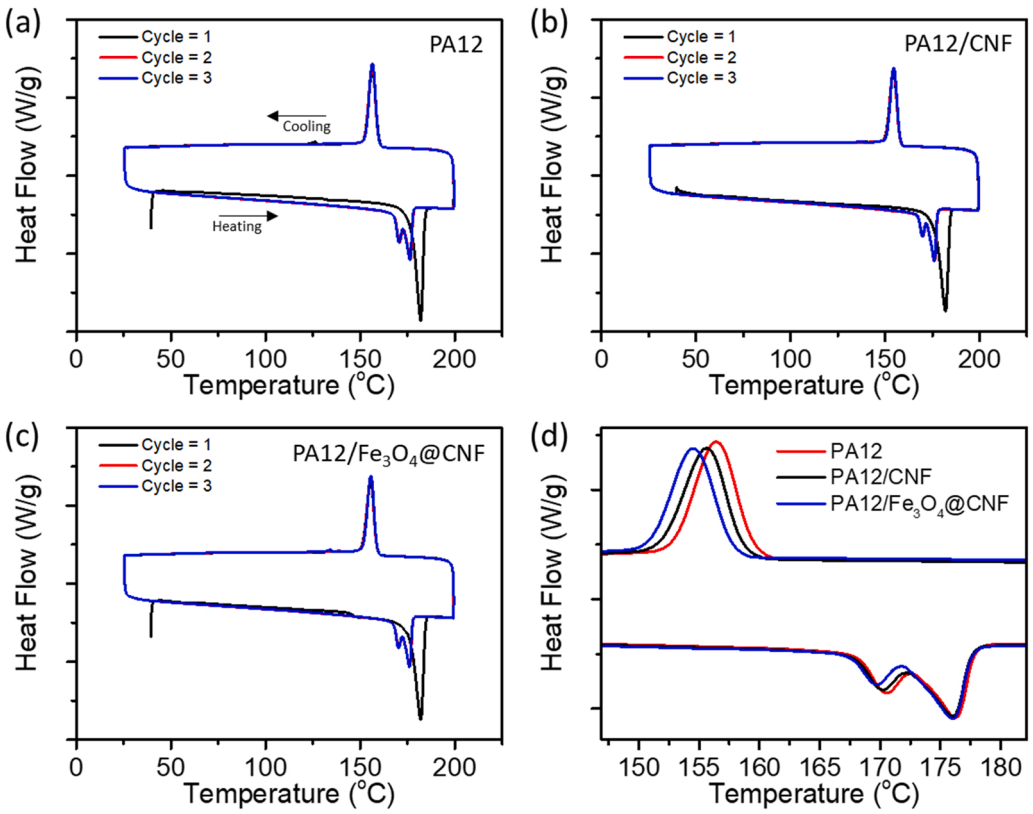

Fig. 6. DSC of (a) PA12, (b) PA12/CNF and (c) PA12/Fe_3O_4 @CNF powders. (d) Comparing the 3rd cycle of each material, a similar melting temperature is observed, but the crystallization temperature decreases from PA12 (156.5 °C) to PA12/CNF (155.5 °C) to PA12/Fe_3O_4@CNF (154.4 °C).

(HRTEM), X-ray diffraction (XRD), Raman spectroscopy and infrared spectroscopy (Fig. 3). Morphology and size of the as-synthesized products is shown in a low magnification TEM image (Fig. 3a). The estimated average size of those particles was 4.3 ± 1.1 nm, as shown in Supporting Information (Fig. S1), while high-resolution TEM (Fig. 3b) shows the D-spacing of 0.316 nm, corresponding to (200) plane (Fig. 3c). A typical XRD pattern of the product is shown in Fig. 3d where all the peaks can be indexed as face centered cubic Fe_3O_4 (JCPDS, No. 19–0629). High purity of the as-synthesized Fe_3O_4 nanoparticles is confirmed by the absence of other diffraction peaks than those related to Fe_3O_4. Broad peaks suggest that the as-synthesized nanoparticles have a reduced crystallinity, being in agreement with the small size observed in TEM (Fig. 3a). Raman spectra in the wavelength range of 200–1000 cm^{-1} were dominated by three peaks located at 318, 517, and 671 cm^{-1} (Fig. 3e), respectively, which are assigned to E_g, $T_{2\,g}$, and $A_{1\,g}$ modes of Fe_3O_4. IR spectrum (Fig. 3 f) shows the stretching Fe-O band of Fe_3O_4 at 586 cm^{-1} (arrow) while other peaks are assigned to the nanoparticle capping layer (i. e. oleylamine and oleic acid) [37].

Preformed nanoparticles were subsequently hybridized with hollow carbon nanofibers (CNF; Fig. S2) as shown in Fig. 2, leading to Fe_3O_4@CNF in which around 85% of the nanoparticles were successfully encapsulated (Fig. 4a-b). Note that the hybridization of CNF with Fe_3O_4 NP produces a black material which is attracted by an external magnetic field (Fig. 4a, inset). Thermogravimetric analysis exhibits at high temperature (i.e. 1000 °C) that Fe_3O_4 @CNF hybrid composite contains 10% iron oxide loading when compared to pristine CNF (Fig. 4c, black). Weight loss around 250 °C is assigned to the decomposition of the surfactant covering the nanoparticles. More importantly, both the morphology (i.e. average size, Fig. S3) and chemical composition of the nanoparticles were retained after the hybridization with hollow carbon nanofibers, as confirmed by powder XRD (Fig. S4), Raman (Fig. 4d) and IR (Fig. S5).

3.2. Preparation of PA12/Fe_3O_4@CNF laser sintering powder

Successful coating of individual polyamide 12 (PA12) powder particles with 0.1 wt% CNF or 0.1 wt% Fe_3O_4@CNF is indicated by the presence of fibers on the surface of the nanocomposites when examined by SEM, which is not present on the uncoated particles (Fig. 5). EDX confirms the presence of Fe in PA12/Fe_3O_4 @CNF (Fig. S6). It is presumed that the Ti detected on the PA12/CNF sample results from titanium dioxide particles, commonly added to PA12 to reduce yellowing when exposed to thermal stress.[25] Furthermore, SEM confirms the coating process did not affect the particle size or shape of the original PA12 powder. This is an important consideration in PBF/LB-P since powder morphology can affect the processability of PBF/LB-P materials and resulting part properties [7]. The particle coating method employed in this work was specifically chosen in order to maintain the near-spherical particle shape of commercially available PA12 which is successfully used in PBF/LB-P.

Ideally, materials for laser sintering have a narrow melting range and no overlap between melting and recrystallization peaks [38]. For both the uncoated and coated powders, a prominent melting and crystallisation peak is observed by DSC (Fig. 6) with clear separation between the two. The melting temperature is similar for the PA12 and PA12/CNF powders. However, the crystallization temperature decreases from PA12 (156.5 °C) to PA12/CNF (155.5 °C) to PA12/Fe_3O_4@CNF (154.4 °C). In previous studies into PBF/LB-P polymer nanocomposites, most have reported an increase in crystallization temperature, presumed to be due to increased heterogeneous nucleation [6,8,39]. However, a few have reported a decrease in crystallization temperature; these have been nanofillers with a plate-like structure and it has been proposed that this is due to a barrier effect where nanofillers hinder the diffusion of polymer molecules and thus reduce the growth of crystals [40–42]. In this study, it is not clear why the crystallization temperature has decreased and will be the subject of future investigations. Nevertheless,

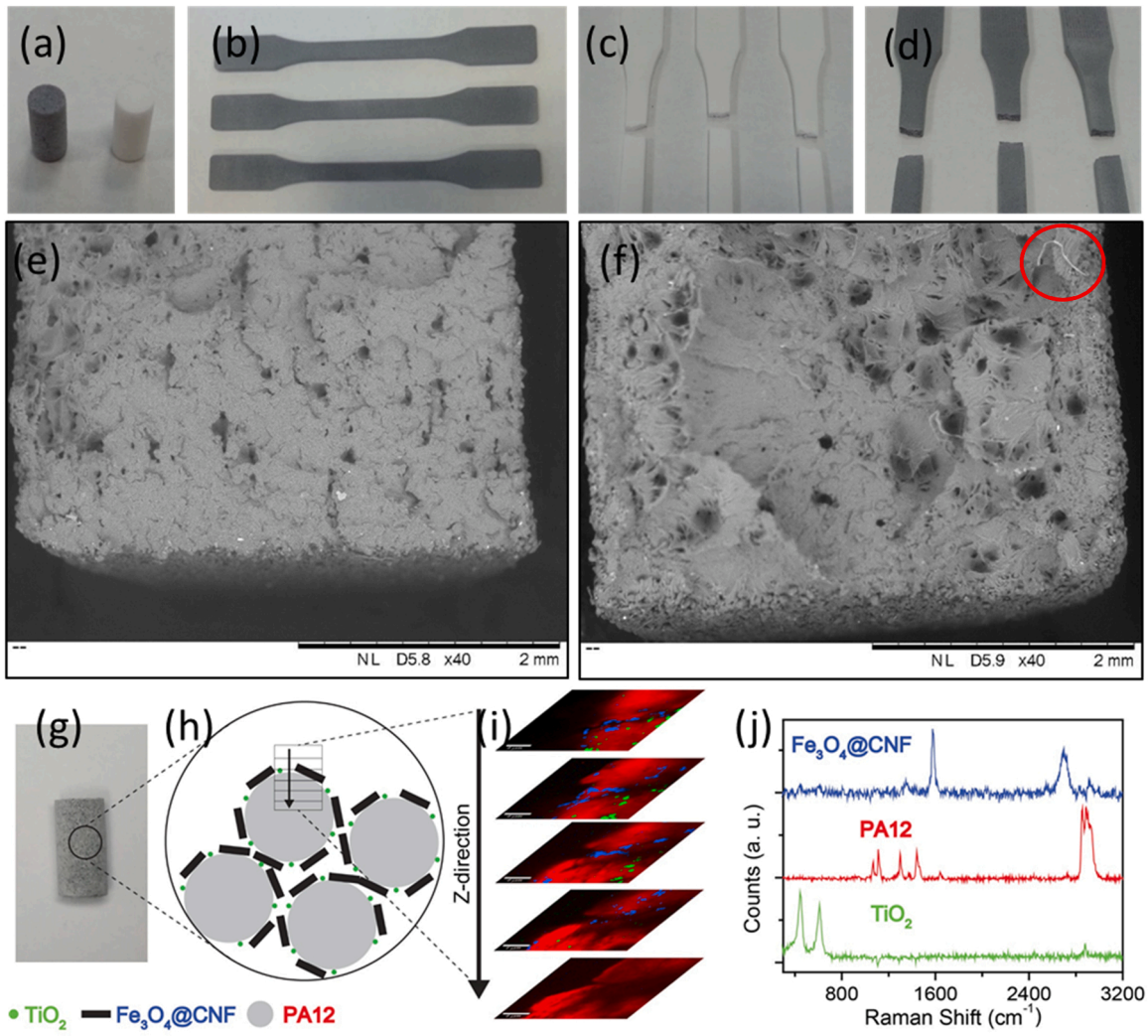

Fig. 7. Structural characterization of PBF/LB-P materials. (a) PA12 (white) and PA12-Fe_3O_4@CNF (dark grey) powders, and (b) PA12-CNF. Images of the fracture of (c) PA12 and (d) PA12-CNF. SEM of fracture surface of (e) PA12 and (f) PA12-CNF, produced at 2500 mm/sec and 21 W, showing good consolidation of both materials. Note the presence of strands (example circled), presumed to be CNF, in the PA12-CNF sample (7 f); (g) PA12-Fe_3O_4@CNF (0.1%wt) cylinder, produced by PBF/LB-P (h) schematic representation, (i) stack of 5 Raman sections (500 nm z-steps) and (j) representative Raman spectra of PA12-Fe_3O_4@CNF (0.1%wt) with Fe_3O_4@CNF (blue), PA12 (red) and TiO_2 (green). Scale bar of (i) 4 μm.

the increase in gap between melting and crystallization temperatures is advantageous in laser sintering since it is generally found to increase the processing window.

3.3. PBF/LB-P of polymer nanocomposite powders

PBF/LB-P was successfully achieved with all three samples powders (i. e. PA12, PA12/CNF and PA12/Fe_3O_4@CNF, Fig. 7). The presence of CNF and Fe_3O_4@CNF did not affect powder spreadability nor did it appear to cause any significant reduction in the processing window of PA12. Similar processing parameters were used successfully for all materials. Whilst establishing a complete process window for each material was out of the scope of this work, the nanocomposites were able to be processed reliably in all combinations between 21 and 25 W laser power and 2000–2500 mm/sec. scan speed, which are commonly used parameters for PA2200. Furthermore, the addition of CNF did not negatively affect the mechanical properties of the PBF/LB-P parts, in fact the PA12-CNF nanocomposites recorded a slightly higher UTS (~8%) and tensile modulus (~5%) (Fig. S7). The increase in modulus (+5%) was not to the same degree as observed in previous work using CNT [8] (+ 48%), which could be related to CNF having a wider diameter than CNT; however, CNF are around 3% the cost of CNT and are thus demonstrated as a promising alternative where additional functionality is required but increased mechanical properties are not as important.

The ability to process the nanocomposite using a range of processing parameters, including those used for commercial PA12, is highly significant since the material is thus less sensitive to machine variances and can be processed using standard parameters without the need for time-consuming parameter searches.

3.4. Characterization of laser sintered parts

Raman punctual spectra shows the presence of polyamide by the band located at 1643 cm^{-1} associated to the C═O stretching band of an amide group (Fig. S8). Moreover, the presence of CNF is confirmed by the peak located at 1590 cm^{-1} (G) which is a result of the vibration of sp^2-bonded carbon in a 2-dimensional hexagonal lattice [43]. Confocal Raman microscopy can be further applied in area mapping mode to provide molecular fingerprints (Raman spectrum) at every pixel with a high lateral resolution (~300 nm) [44]. Hence, it is confirmed that Fe_3O_4@CNF (Fig. S9a, blue) are distributed along the surface of PA12 (Fig. S9a, red) within an area of 20 × 20 μm^2. Note that Fe_3O_4 nanoparticles are not observed in the Raman spectrum due to the low loading (10% in the CNF) and their small size. In contrast, large TiO_2

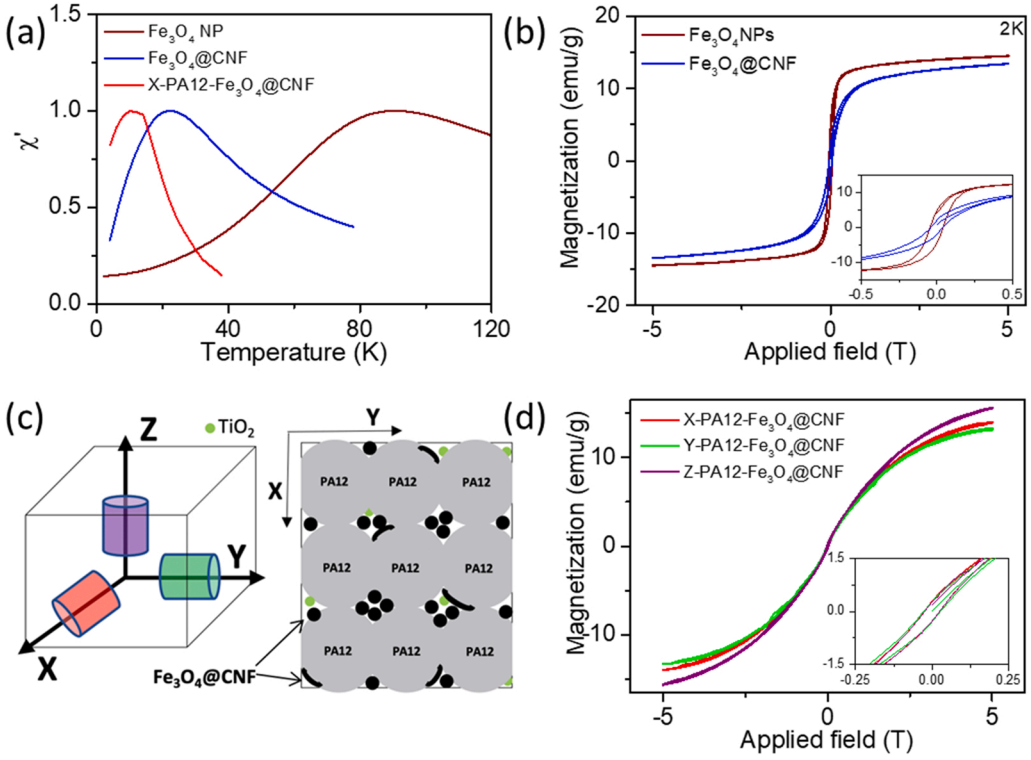

Fig. 8. (a) In-phase AC susceptibility versus temperature at 1 Hz of Fe_3O_4 (brown), Fe_3O_4@CNF (blue) and PBF/LB-P PA12-Fe_3O_4@CNF composite along X-axis (red). (b) Magnetic hysteresis of Fe_3O_4 (brown) and Fe_3O_4 @CNF (blue) at 2 K. (c) PA12-Fe_3O_4@CNF cylinder parts produced by PBF/LB-P (Fig. 7a) built in three orientations with alignment of the long symmetry axis along the X (red), Y (green) and the Z (purple) axes of the build chamber, and different views of the XY cross-section of the Z-cylinder showing the preferential alignment of Fe_3O_4@CNF, and (d) their respective saturation magnetization (inset: zoom of the hysteresis loops at low magnetic fields).

nanoparticles, which are added to commercial polyamide powders to reduce their susceptibility to yellowing when exposed to thermal stress during PBF/LB-P, were detected (Fig. S9a, green) [45]. Volumetric Z-stack of XY-images, depicted in Fig. S9b-f, were collected within the same area 20 × 20 μm^2 as Raman can penetrate through the sample, providing information not only from the superficial distribution (general mapping as shown above) but also the interface [46]. As expected, Fe_3O_4@CNF are mostly located on the surface of the PA12 nanoparticles as no signal is detected in the most interior layers (Fig. S9f).

Similar analysis protocol was applied to a different PA12 nanoparticle within the same PA12-Fe_3O_4@CNF material processed by PBF/LB-P and reveals similar behavior, suggesting that Fe_3O_4@CNF is homogeneously distributed on the PBF/LB-P composite (Fig. 7i-j). It is worth stressing that Raman measurements were carried out directly on the PBF/LB-P material as this technique does not require sample preparation (i.e. use of stains) [47] and it is non-destructive (i.e. ultramicrotomy) [48], gaining molecular information of the real composite.

A common concern in polymer nanocomposites is agglomeration; however, as each individual PA12 particle is coated with a small amount of Fe_3O_4@CNF and only the surface of the particle has been melted by the laser, it is reasonable to presume that an evenly structured network of nanoparticles is present throughout the PBF/LB-P part.

3.5. Magnetic investigations of PA12-Fe_3O_4@CNF (0.1%wt) parts produced by PBF/LB-P

The magnetic properties of PA12-Fe_3O_4@CNF cylindric parts produced by PBF/LB-P (built in three orientations with alignment of the long symmetry axis along the X, Y and the Z axes of the build chamber, respectively) were investigated using a commercial SQUID (superconducting quantum interference device) magnetometer. To ascertain any possible effects from PBF/LB-P, the magnetic behavior of the preformed Fe_3O_4 nanoparticles and the Fe_3O_4@CNF hybrid material in direct (DC) and alternating current (AC) mode were first carefully analyzed. As shown in Fig. 8a, both Fe_3O_4 and Fe_3O_4@CNF exhibited an in-phase signal of the AC susceptibility at 1 Hz under zero DC field that is associated with the blocking temperature from the superparamagnetic to the ferromagnetic transition with decreasing temperature. As recently demonstrated by our group [23], the formation of Fe_3O_4@CNF by hybridization of preformed Fe_3O_4 nanoparticles with CNF reduces significantly the blocking temperature of iron nanoparticles (from 61 to 16 K), which is in line with the shift observed in the zero-field-cooled (ZFC) – field cooled (FC) measurements (Fig. S10). Such decrease was associated to the dispersion of the nanoparticles on the corrugated surfaces of carbon nanofibers as no noticeable changes in nanoparticle size visible by transmission electron microscopy after hybridization (Figs. 4b and S3). [49]. Moreover, it was also observed that the hybridization of Fe_3O_4 nanoparticles with CNF modifies their behaviour from interacting (Fe_3O_4, Fig. S11) to non-interacting systems (Fe_3O_4@CNF, Fig. S12) based on the variations observed in the blocking temperature within the 1–1000 Hz frequency range (Fig. S13–14) [33,50]. The blocking temperature observed for a laser sintered cylinder (X-PA12-Fe_3O_4@CNF) as the peak maximum of the in-phase AC susceptibility signal is slightly smaller than the one observed for Fe_3O_4@CNF (Fig. 8a). This indicates that the Fe_3O_4 nanoparticles in CNF do not aggregate or grow after laser sintering, demonstrating the suitability of the methodology employed for protecting the magnetic functionality of magnetic nanoparticles.

Magnetic hysteresis loops for Fe_3O_4 and Fe_3O_4@CNF were measured below (i.e. 2 K) and above (i.e. 300 K) the blocking temperature. As shown in Fig. 8b, the hysteresis loop at 2 K confirms that the samples are ferromagnetic below the blocking temperature, due to the presence of coercivity and remanence (Fig. 8b, inset). In contrast, the lack of coercivity and remanence observed at 300 K (Fig. S15) indicates that the Fe_3O_4 nanoparticles have superparamagnetic properties above the blocking temperature, meaning that Fe_3O_4 nanoparticles respond to an external magnetic field at room temperature but they don't retain any residual magnetism when the external magnetic field is removed [51]. As a result of confinement of Fe_3O_4 in CNF, a slightly lower coercive field is observed, whereas no changes on the saturation magnetization values at 2 K were noticed. When comparing with the cylindrical PA12-Fe_3O_4@CNF parts built along the X (red), Y (green) and the Z (purple) axes of the chamber (Fig. 8c), the cylindric part built along the

Table 1
Summary of the magnetic parameters for preformed Fe_3O_4 free-standing (Fe_3O_4NP), hybridized with CNF (Fe_3O_4@CNF) and sintered with PA12 given rise to composite cylindrical parts built in three orientations with alignment of the long symmetry axis along the X (X-PA12-Fe_3O_4@CNF), Y (Y-PA12-Fe_3O_4@CNF) and the Z (Z-PA12-Fe_3O_4@CNF) axes.

	Fe_3O_4NP	Fe_3O_4@CNF	X-PA12-Fe_3O_4@CNF	Y-PA12-Fe_3O_4@CNF	Z-PA12-Fe_3O_4@CNF
$T_{ZFC\text{-}peak}$ [K]	66	18.3	-	-	-
T_B (max of X′ peak at 1 Hz)[K]	91	22	12	-	-
$M_{2\,K}$ [emu g^{-1}] (at 5 T)	14.5	13.44	14	13.3	15.6
H_c at 2 K [mT]	86.2 (−45.2/41)	77.4 (−39.5/37.9)	50.7 (−26.1/24.6)	54.7 (−27.7/27)	48.55 (−24.45/24.1)

Z-axis reaches saturation values of the magnetization faster than the other two (X and Y) suggesting that the Fe_3O_4@CNF hybrids are preferentially aligned along the Z-axis after laser sintering (Fig. 8d). Similar values for the coercive field are observed along the different directions. This result opens up the possibility of manufacturing PBF/LB-P pieces showing an easy magnetization direction.

To the best of our knowledge, there have been no previous studies in the development of a magnetic PBF/LB-P composite using Fe_3O_4@CNF hybrids. Bin *et al.* presented a magnetic laser-sintered composite made of Fe_3O_4 nanoparticles but it was in the absence of carbon nanostructures and using a poly-L-lactic acid (PLLA) scaffold [52]. Despite the high iron loading (9%), the magnetic composite exhibited a lower saturation magnetization (i. e. 6.1 emu/g) at room temperature in comparison to our work, which can be related to the agglomeration of nanoparticles. Our method has addressed previously encountered issues with control of the final morphology and chemical composition of the nanoparticles [21,22], and agglomeration [22,52], important parameters that determine magnetic parameters. Our method has also improved the physical properties of the sintered composite, recording a slightly higher UTS (~8%) and tensile modulus (~5%) (Fig. S7). In previous work looking at magnetic PBF/LB-P of magnetic powders, mechanical properties have not been reported, and it is therefore speculated that agglomeration may have had a negative effect.(Table 1).

4. Conclusions

In this work, a quick and easy method for adding functionality to commercial PA12 PBF/LB-P powders has been successfully demonstrated. By coating individual powder particles with CNF filled with metal oxide particles, a polymer with magnetic properties has been produced. This method has successfully allowed the protection of the functionality of the magnetic nanoparticles avoiding aggregation and nanoparticle growth, which is a challenge within the area. Moreover, the observance of the preferred alignment of the Fe_3O_4@CNF hybrids along a direction after PBF/LB-P opens up the possibility of manufacturing PBF/LB-P pieces showing an easy magnetization direction.

With the metal oxide particles being encapsulated within the CNF structure, and the CNF having no negative affect on the processing window, it is proposed that the method could be adapted for a range of other functionalities simply by changing the nanoparticle within the CNF structure. This is particularly significant in PBF/LB-P where the cost of producing powders in small quantities is expensive, and the process of establishing a processing window for each new material is time consuming.

CRediT authorship contribution statement

Ruth D. Goodridge: Writing – review & editing, Writing – original draft, Visualization, Validation, Supervision, Resources, Project administration, Methodology, Investigation, Funding acquisition, Formal analysis, Data curation, Conceptualization. **Carlos Herreros-Lucas:** Writing – review & editing, Writing – original draft, Visualization, Validation, Methodology, Investigation, Formal analysis, Data curation. **Maria del Carmen Gimenez-Lopez:** Writing – review & editing, Visualization, Validation, Supervision, Resources, Project administration, Methodology, Investigation, Funding acquisition, Formal analysis, Data curation, Conceptualization.

Declaration of Competing Interest

The authors declare the following financial interests/personal relationships which may be considered as potential competing interests: Ruth Goodridge has patent #2211110.8 pending to University of Nottingham.

Data availability

Data will be made available on request.

Acknowledgements

This work was supported by the Engineering and Physical Sciences Research Council [grant number EP/I033335/2], the Ministry of Science of Spain (Projects No. RTI2018–101097-A-I00, PID2021–127341OB-I00, TED2021-131451B-C21, PDC2022-133925-I00 and RyC-2016–20258 for M. G-L), the European Research Council (ERC) (Starting Investigator Grant (NANOCOMP-679124) for M.G-L) and the Xunta de Galicia (Centro singular de investigación de Galicia accreditation 2019–2022, ED431G 2019/03) and the European Union (European Regional Development Fund - ERDF). The authors would like to thank Ezequiel Vazquez-Fernandez for technical assistance with Raman, Nicola Weston for her assistance with TEM and Mark East for his support with laser sintering.

Appendix A. Supporting information

Supplementary data associated with this article can be found in the online version at doi:10.1016/j.addma.2023.103518.

References

[1] I. Gibson, D. Rosen, B. Stucker, Addit. Manuf.Tech., Springer-Verlag,, New York, 2015.
[2] R. Goodridge, S. Ziegelmeier, in: M.Brandt (Ed.), Woodhead Publishing Series in Electronic and Optical Materials, Laser Additive Manufacturing, Woodhead Publishing, 2017, pp. 181–204.
[3] R.D. Goodridge, C.J. Tuck, R.J.M. Hague, R.J.M. Progress, Mater. Sci. 57 (2) (2012) 229.
[4] A. Wegner, Dissertation, Universität Duisburg-Essen, 2015.
[5] G.V. Salmoria, R.A. Paggi, A. Lago, V.E. Beal, Polym. Test. 30 (6) (2011) 611.
[6] Y. Chunze, S. Yusheng, Y. Jinsong, L. Jinhui, J. Reinf. Plast. Compos. 28 (23) (2009) 2889.
[7] R.D. Goodridge, M.L. Shofner, R.J.M. Hague, M. McClelland, M.R. Schlea, R. B. Johnson, C.J. Tuck, Polym. Test. 30 (1) (2011) 94.
[8] J. Bai, R.D. Goodridge, R.J.M. Hague, M. Song, Polym. Eng. Sci. 53 (9) (2013) 1937.
[9] J. Bai, R.D. Goodridge, R.J.M. Hague, M. Song, H. Murakami, J. Mater. Res. 29 (17) (2014) 1817.
[10] D. Drummer, S. Greiner, M. Zhao, K. Wudy, Addit. Manuf. 27 (2019) 379.
[11] D. Hui, R.D. Goodridge, C.A. Scotchford, D.M. Grant, Addit. Manuf. 22 (2018) 560.
[12] O.N. Metelkina, R.W. Lodge, P.G. Rudakovskaya, V.M. Gerasimov, C. Herreros Lucas, I.S. Grebennikov, I.V. Shchetinin, A.G. Savchenko, G.E. Pavlovskaya, G.

A. Rance, M. del Carmen Gimenez-Lopez, A.N. Khlobystov, A.G. Majouga, J. Mater. Chem. C. 5 (2017) 2167–2174.
[13] A. La Torre, G.A. Rance, S.A. Miners, C. Herreros Lucas, E.F. Smith, M.W. Fay, T. Zoberbier, M.C. Giménez-López, U. Kaiser, P.D. Brown, A.N. Khlobystov, Nanotechnology 27 (2016), 175604.
[14] M. Aygün, M. Guillen-Soler, J.M. Vila-Fungueiriño, A. Kurtoglu, T.W. Chamberlain, A.N. Khlobystov, M. del Carmen Gimenez-Lopez, ChemSusChem 14 (2021) 4973–4984.
[15] A. La Torre, M. del Carmen Gimenez-Lopez, M.W. Fay, C. Herreros Lucas, P. D. Brown, A.N. Khlobystov, Small 11 (2015) 2756–2761.
[16] M. del Carmen Gimenez-Lopez, A. Kurtoglu, D.A. Walsh, A.N. Khlobystov, Adv. Mater. 28 (2016) 9103–9108.
[17] A. Masotti, A. Caporali, Int. J. Mol. Sci. 14 (2013) 24619.
[18] H. Wang, K.-Y. Lin, B. Jing, G. Krylova, G.E. Sigmon, P. McGinn, Y. Zhu, C. Na, Water Res. 47 (12) (2013) 4198.
[19] A. Rajan, M. Sharma, N.K. Sahu, Sci. Rep. 10 (2020) 15045.
[20] H. Wu, O. Wang, Y. Tian, M. Wang, B. Su, C. Yan, K. Zhou, Y. Shi, ACS Appl. Mater. Interfaces 13 (2021) 12679–12688.
[21] T. Hupfeld, S. Salamon, J. Landers, A. Sommereyns, C. Donate-Buendia, J. Schmidt, H. Wende, M. Schmidt, S. Barcikowski, B. Gokce. J. Mat. Chem. C. 35 (2020).
[22] B. Dusenberg, P. Groppe, S. Mussig, J. Schmidt, A. Buck, Polymers 14 (2022) 4178.
[23] L. Vizcaíno-Anaya, C. Herreros-Lucas, J.M. Vila-Fungueiriño, M. del Carmen Giménez-López, Eur. J. Chem. 28 (2022), e202201861.
[24] H. Liu, K. Moon, J. Li, Y. Xie, J. Liu, Z. Sun, L. Lu, Y. Tang, C. Wong, Nano Energy 77 (2020), 105058.
[25] R. Madhuvilakku, Y. Yen, W. Yan, G. Huang 7 (2022) 15936–15950.
[26] A. La Torre, M. del Carmen Giménez-López, M.W. Fay, G.A. Rance, W. A. Solomonsz, T.W. Chamberlain, P.D. Brown, A.N. Khlobystov, ACS Nano 6 (2012) 2000–2007.
[27] S. Sun, H. Zeng, J. Am. Chem. Soc. 124 (28) (2002) 8204.
[28] Y. Yang, M. Huang, J. Qian, D. Gao, X. Liang, Sci. Rep. 10 (2020) 8331.
[29] Q. Li, C.W. Kartikowati, S. Horie, T. Ogi, T. Iwaki, K. Okuyama, Sci. Rep. 7 (2017) 9894.
[30] C.L. Roman, N. da Silva Moura, S. Wicker, K.M. Dooley, J.A. Dorman, ACS Appl. Nano Mater. 5 (2022) 3676–3685.
[31] I. Castellanos-Rubio, O. Arriortua, D. Iglesias-Rojas, A. Barón, I. Rodrigo, L. Marcano, J.S. Garitaonandia, I. Orue, M. Luisa Fdez-Gubieda, M. Insausti, Chem. Mater. 33 (2021) 8693–8704.
[32] F.B. Effenberger, R.A. Couto, P.K. Kiyohara, G. Machado, S.H. Masunaga, R.F. Jardim, L.M. Rossi, 2017, 28, 115603.
[33] M.C. Gimenez-Lopez, A. La Torre, M.W. Fay, P.D. Brown, A.N. Khlobystov, Angew. Chem. 52 (7) (2013) 2051.
[34] J. Santoyo Salazar, L. Perez, O. de Abril, L. Truong Phuoc, D. Ihiawakrim, M. Vazquez, J. Greneche, S. Begin-Colin, G. Pourroy, Chem. Mater. 23 (2011) 1379–1386.
[35] A. Rajan, N. Kumar Sahu, ACS Appl. Nano Mater. 4 (2021) 4642–4653.
[36] V. Alimohammadi, S.A. Seyyed Ebrahimi, F. Kashanian, Z. Lalegani, M. Habibi-Rezaei, B. Hamawandi, Green. Synth., Funct., Charact. (2022) 8.
[37] S. Chang, C. Liu, Y. Sun, Z. Yan, X. Zhang, X. Hu, H. Zhang, ACS Appl. Nano Mater. 3 (3) (2020) 2302.
[38] J.P. Kruth, G. Levy, F. Klocke, T.H. Childs, CIRP Ann. 56 (2) (2007) 730.
[39] M. Van Den Eynde, PhD Thesis, KU Leuven, 2018.
[40] L.J. Tan, W. Zhu, K. Zhou, Powder Technol. 369 (2020) 25.
[41] Y. Jin, N. Chen, Y. Li, Q. Wang, RSC Adv. 10 (35) (2020) 20405.
[42] B.O. Sivadas, I. Ashcroft, A.N. Khlobystov, R.D. Goodridge, Adv. Ind. Eng. Polym. Res. 4 (4) (2021) 277.
[43] B. Zhumadilov, G. Partizan, B. Medyanova, A. Kenzhegulov, G. Suyundykova, B. Aliyev, Mater. Today.: Proc. 31 (2020) 412–416.
[44] M. Felhofer, B. Prats-Mateu, P. Bock, N. Gierlinger, Tree Physiol. 38 (10) (2018) 1526.
[45] F.-E. Baumann, S..Monsheimer, M..Grebe, W..Christoph, T..Schiffer, H..Scholten. US 7,148,286 B2, 2006.
[46] M.B. Albro, M.S. Bergholt, J.P. St-Pierre, A. Vinals Guitart, H.M. Zlotnick, E. G. Evita, M.M. Stevens, Regen. Med 3 (2018) 3.
[47] B. Situ, X. Ye, Q. Zhao, L. Mai, Y. Huang, S. Wang, J. Chen, B. Li, B. He, Y. Zhang, J. Zou, B.Z. Tang, X. Pan, L. Zheng, Adv. Sci. 7 (4) (2020), 1902760.
[48] I. Andreu, A. Urtizberea, E. Natividad, Nanoscale 12 (2020) 572.
[49] M.D. Nguyen, H.-V. Tran, S. Xu, T.R. Lee, Appl. Sci. 11 (23) (2021) 11301.
[50] V.B. Barbeta, R.F. Jardim, P.K. Kiyohara, F.B. Effenberger, L.M. Rossi, J. Appl. Phys. 107 (2010), 073913.
[51] W. Lu, Y. Shen, A. Xie, W. Zhang, J. Magn. Magn. Mater. 322 (13) (2010) 1828.
[52] S. Bin, A. Wang, W. Guo, L. Yu, P. Feng, Polymers 12 (2020) 2045.